NANO LETTERS

Letter

pubs.acs.org/NanoLett

Self-Assembled Organic Nanowires for High Power Density Lithium Ion Batteries

Chao Luo,[†,§] Ruiming Huang,[‡,§] Ruslan Kevorkyants,[‡] Michele Pavanello,[‡] Huixin He,*[,‡] and Chunsheng Wang*[,†]

[†]Department of Chemical and Biomolecular Engineering, University of Maryland, College Park, Maryland 20742, United States

[‡]Department of Chemistry, Rutgers University, Newark, New Jersey, 07102, United States

Supporting Information

ABSTRACT: The electroactive organic materials are promising alternatives to inorganic electrode materials for the new generation of green Li-ion batteries due to their sustainability, environmental benignity, and low cost. Croconic acid disodium salt (CADS) was used as Li-ion battery electrode, and CADS organic wires with different diameters were fabricated through a facile synthetic route using antisolvent crystallization method to overcome the challenges of low electronic conductivity of CADS and lithiation induced strain. The CADS nanowire exhibits much better electrochemical performance than its crystal bulk material and microwire counterpart. CADS nanowire with a diameter of 150 nm delivers a reversible capability of 177 mAh g^{-1} at a current density of 0.2 C and retains capacity of 170 mAh g^{-1} after 110 charge/discharge cycles. The nanowire structure also remarkably enhances the kinetics of croconic acid disodium salt. The CADS nanowire retains 50% of the 0.1 C capacity even when the current density increases to 6 C. In contrast, the crystal bulk and microwire material completely lose their capacities when the current density merely increases to 2 C. Such a high rate performance of CADS nanowire is attributed to its short ion diffusion pathway and large surface area, which enable fast ion and electron transport in the electrode. The theoretical calculation suggests that lithiation of CADS experiences an ion exchange process. The sodium ions in CADS will be gradually replaced by lithium ions during the lithiation and delithiation of CADS electrode, which is confirmed by inductively coupled plasma test.

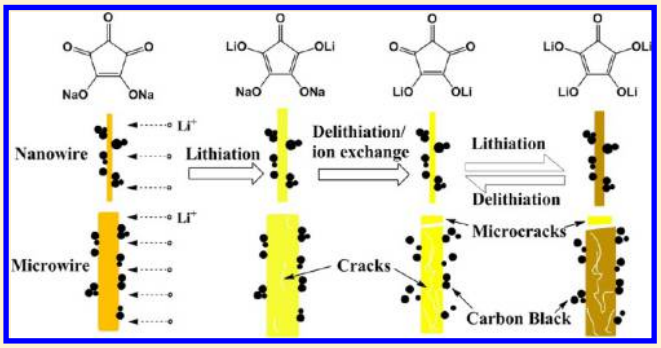

KEYWORDS: *Lithium ion battery, croconic acid disodium salt, organic nanowire, antisolvent crystallization synthesis, high power density*

Lithium ion batteries, the best power sources for portable electronics, are considered as the most promising energy storage devices for emerging electric vehicles and smart grids.[1,2] Currently, lithium ion batteries largely rely on inorganic compounds as electrodes such as $LiCoO_2$ and $LiFePO_4$.[3−6] Most of these compounds are synthesized using nonearth-abundant resources via energy-demanding ceramic processes.[7] Recycling of used batteries further consumes large quantities of energy and chemicals, releasing more CO_2. To satisfy the urgent demand for rechargeable energy storage devices in electric vehicles and smart grids, next generation battery electrodes should be made from renewable or recyclable resources via low energy consumption processes. One possible approach is to use biomass or recyclable organic materials as electrode materials via solution phase routes.[8] In addition, most of organic compounds are degradable, so the organic electrode materials are environmentally benign.

Recently, carbonyl group based organic materials such as purpurin,[9] tribrominated trioxotriangulene,[10] perylenetetracarboxylic anhydride,[11] and other compounds[12−23] have been investigated as electrodes for Li-ion batteries, and some organic materials can also been used for Na-ion battery electrodes.[24,25] However, due to dissolution of organic compounds in electrolyte and very low electrical conductivity, the electrochemical performance of these sustainable organic electrode materials is much worse than their inorganic counterparts. The solubility of organic compounds could be reduced by enhancing their polarities via salt formation[26] and solubility of organic salt in organic electrolyte can be further reduced by increasing the concentration of lithium salt in organic electrolyte that has effectively suppressed dissolution of polysulfide in lithium sulfur batteries.[27] Although use of organic salts such as lithium salt of tetrahydroxybenzoquinone[28] can mitigate the dissolution issue,[7] the low electronic conductivity of organic salts and volume change during lithiation/delithiation still limits the power density and cycling stability of organic electrodes. Because of the very low electrical

Received: January 3, 2014
Revised: February 13, 2014
Published: February 18, 2014

conductivity of most organic compounds, up to 30 wt % of conductive carbon black is normally mixed into organic electrode to provide electron pathways for the electrochemical reactions and another ~5−10% (by weight) nonconductive polymer binders are also needed to mechanically bind all the components into an electrode. Even adding 30 wt % of carbon black, there is only a portion of active material contributes to the output power of a battery in organic electrodes due to large size of organic salt particles. A recent work of organic $Li_4C_8H_2O_6$ nanosheets for Li-ion batteries has demonstrated that nanosheet structure provides short Li-ion diffusion pathways and large contact areas for both conductive carbon and electrolyte, leading to high rate capability.[29]

In this study, croconic acid disodium salt (CADS) wires are used as models to investigate the size effect on the battery performance of organic electrodes. CADS has a cyclopentene backbone with three carbonyl groups, and two of them are connected by a conjugated chemical bond as shown in Scheme 1. The two carbonyl groups in CADS can participate in the reversible reaction with lithium ions,[8] providing a theoretical capacity of 288 mAh g^{-1}. According to the reported reaction mechanism for carbonyl group based organic electrodes, only carbonyl groups that are connected by conjugated structure such as carbon−carbon double bond or benzene ring can participate in the lithiation reaction.[26] There are three carbonyl groups in CADS. Only two of them are connected by conjugated structure, thus active for the lithiation reaction. In addition, the specific capacity of CADS nanowire shown in Figure 5 also supports the reaction mechanism. The specific capacity of CADS nanowire is 200 mAh g^{-1} at a low current density of 0.1 C, which is close to the theoretical capacity (288 mAh g^{-1}) of CADS based on lithiation reaction of two carbonyl groups. CADS wires with diameter size ranging from 150 nm to 4 μm were synthesized by antisolvent crystallization method to reduce the strain and Li-ion diffusion length. The 150 nm CADS nanowires exhibit superior capacity, rate capability, and cycling stability. The theoretical calculation for lithiation and delithiation of CADS suggests that sodium ions in CADS will be gradually replaced by lithium ions during the lithiation and delithiation of CADS electrode, which is confirmed by inductively coupled plasma test. Because Li croconate has a more stable crystal structure than Na croconate, the formation of Li croconate further enhances the cycling stability of CADS electrode. To our best knowledge, CADS nanowires demonstrate one of the best battery performances for reported organic compounds in terms of cycling stability and rate performance at a low carbon content.[16]

Scheme 1. Molecular Structure of Croconic Acid Disodium Salt

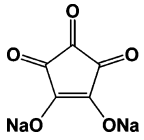

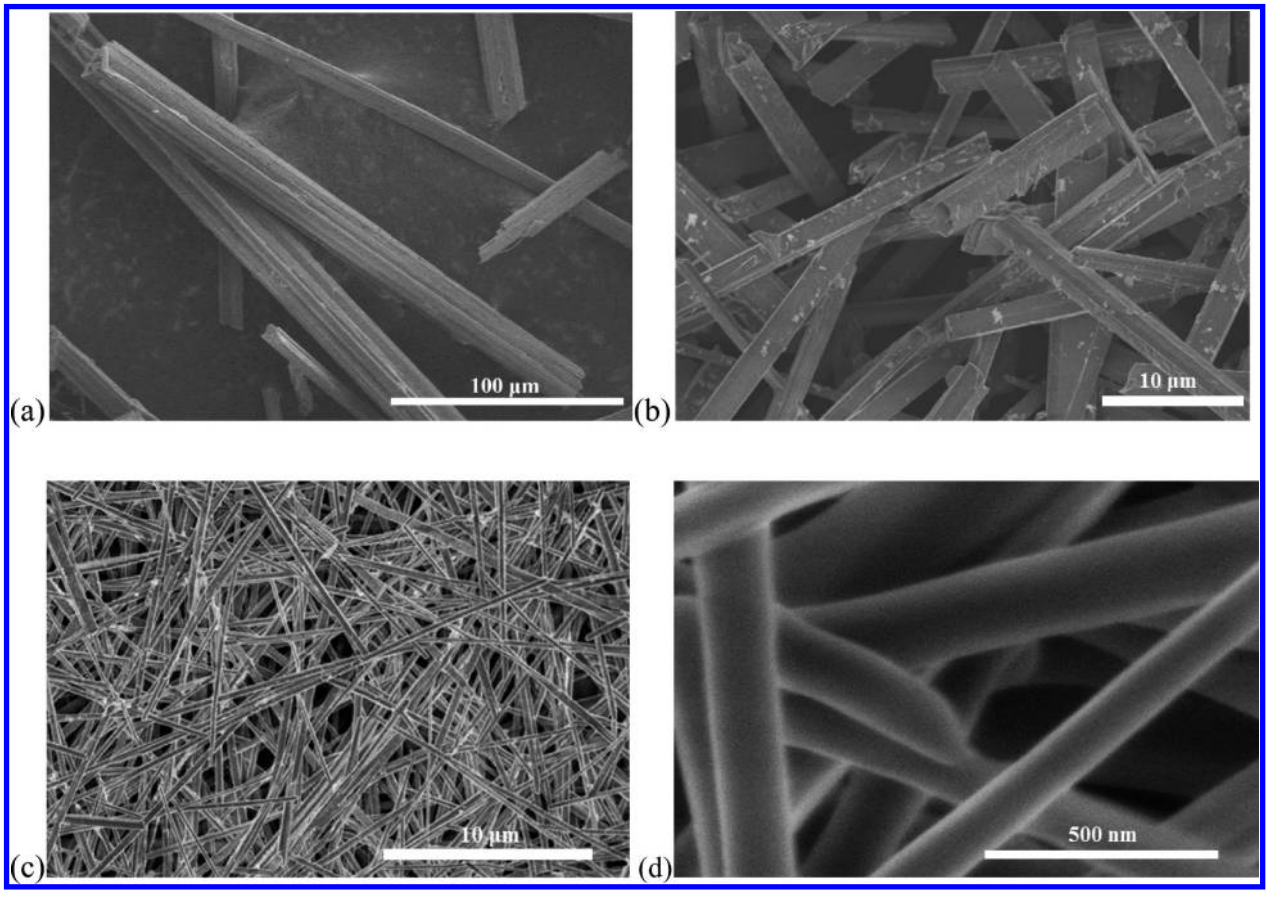

Figure 1. SEM images for CADS micropillar (a), CADS microwire (b), and CADS nanowire (c,d).

dx.doi.org/10.1021/nl500026j | *Nano Lett.* 2014, 14, 1596−1602

Crystal CADS micropillars with the width of 10 μm and length longer than 100 μm (Figure 1a) were prepared by directly recrystallizing CADS from water and are used as control samples. Because of the insulating nature of CADS, the large particle size will significantly increase the transport resistance of Li-ion and electron in the CADS micropillars. The large size and small surface area of CADS micropillar also results in poor contact between CADS and conductive carbon, thus remarkably reducing the reaction kinetics. To improve the lithiation/delithiation kinetics, CADS microwires with an average diameter about 4 μm (Figure 1b) and CADS nanowires with a mean diameter about 150 nm (Figure 1c,d) were fabricated at room temperature using antisolvent crystallization method. The growth of CADS nanowires is driven by the reduction of the solubility of CADS when CADS aqueous solution is added into acetone (a poor solvent for CADS). Under bath sonication, CADS starts to crystallize within a few minutes due to the poor solubility in the water/acetone mixture solvent and self-assemble into nanowires, which is possibly due to $\pi-\pi$ interaction between CADS molecules.[30] The CADS wires synthesized by antisolvent crystallization method have very uniform diameters (Figure 1b,c). The diameter of CADS wires can be manipulated by tuning the concentration of CADS in aqueous solution. The lower concentration CADS aqueous solution yields thinner CADS nanowires.

The crystal structures of three CADS samples are identified by X-ray diffraction (XRD). The XRD patterns in figure 2 reveal that the CADS micropillar, CADS microwire, and CADS nanowire have the same crystal structure. No impurity peak is observed in all three CADS samples. The peak intensity of CADS nanowire is stronger than that of CADS micropillar and CADS microwire, demonstrating that CADS nanowires have high crystallinity and relatively uniform crystal size.

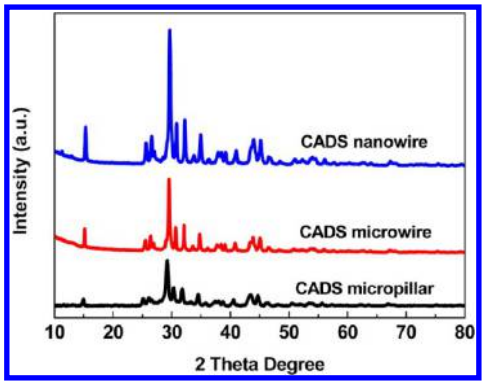

Figure 2. XRD patterns of CADS micropillar, CADS microwire, and CADS nanowire.

The charge and discharge profiles for CADS micropillar, CADS microwire, and CADS nanowire in the second cycle were measured at a current density of 0.2 C (1 C is defined as 288 mA g^{-1}) and are shown in Figure 3a. The lithiation potential decreases and delithiation potential increases with the size of CADS nanowire increases from 150 nm to 4 μm and then to 10 μm. The cyclic voltammograms (CV) of three CADSs with different diameter in Figure 3b–d shows a peak at 1.6 V with a small shoulder at 2.1 V during lithiation, and a peak at 2.0 V with a small shoulder at 2.6 V during delithiation, demonstrating that CADS undergoes a two-step reaction with lithium ions. The two carbonyl groups connected by carbon–carbon double bond react with lithium ions step by step. The potential hysteresis (ΔV) between the cathodic peak and anodic peak is 0.62 V for CADS micropillar, 0.47 V for CADS microwire, and 0.30 V for CADS nanowire, indicating that the overpotential of CADS nanowire is smaller than CADS micropillar and CADS microwire. The increase of potential hysteresis with wire size confirms that lithiation/delithiation kinetics decreases with the increase of wire size. The equilibrium potentials of CADS are estimated by averaging the lithiation and delithiation potential. The equilibrium lithiation potentials of CADS are 1.8 and 2.35 V. As shown in CV curves in Figure 3, the lithiation peak potential slightly increases to more positive value with lithiation and delithiation cycles. To explore the mechanism for two-step reaction and potential shift, the first principle DFT calculation is applied to better understand the lithiation process. Table S1 in the Supporting Information collects the values of the total electronic bonding energy of various species involved in the reduction of CADS. Supporting Information Table S2 collects the calculated reduction potential of the CADS with respect to a lithium electrode potential. Figure 4 schematically reports the energy levels of Na and Li croconate for the three reduced forms considered. The potentials in Supporting Information Table S2 indicate that the one-electron and the two-electron reduction of CADS occur at very similar potentials. The sequential one-electron reductions are estimated to be 2.42 and 2.36 V, which is higher than the equilibrium potential demonstrated by CV scans (2.35 and 1.8 V). The large potential difference (2.36 − 1.8 = 0.56 V) in second step reaction is probably attributed to the strain overpotential induced by the volume expansion at high lithiation levels. A large strain overpotential of 0.6 V was reported for lithiation of Sn.[31] Because of the low strain at low lithiation level, the calculated potential in the first step reaction is similar to measured potential in CV. However, the calculations are unable to ascertain whether the electrochemical potentials are due to a concerted two-electron process or two sequential one-electron processes. Analyzing the overall stability of the sodium and lithium croconate indicates (see Supporting Information Table S1) that lithium croconate forms a more stable crystal than the sodium salt. Thus, it is possible that the CADS undergoes a chemical exchange from sodium croconiate to lithium croconate. For this reason, additional simulations were carried out for the reduction of lithium croconate. The simulations show that the reduction potential for lithium croconate is 2.56 and 2.49 V for the single one-electron processes, respectively. Thus, if a counterion exchange occurs during the CV scans, the reduction potential should slightly increases, which is in well agreement with CV scans in Figure 3. The simulations qualitatively reproduce the potentials determined experimentally and predict a possible sodium–lithium exchange during the lithiation and delithiation of CADS electrode. Such a prediction is further confirmed by inductively coupled plasma (ICP) test. A fresh CADS electrode and a CADS electrode after first cycle are dissolved in water separately, and then Li^+ and Na^+ concentration in water was measured by ICP. The result shows that the concentrations of Li^+ and Na^+ in fresh electrode are 0 and 0.135 mg L^{-1}, respectively, while the concentrations of Li^+ and Na^+ in cycled electrode are 0.103 mg L^{-1} and 0.020 mg L^{-1}, demonstrating that most of sodium ions in CADS are exchanged by lithium ions.

The formation and growth of solid electrolyte interphase (SEI) layer on the surface of CADS is also evidenced by CV in Figure 3b–d. A sharp peak at 0.8 V in the first anodic scan

dx.doi.org/10.1021/nl500026j | Nano Lett. 2014, 14, 1596–1602

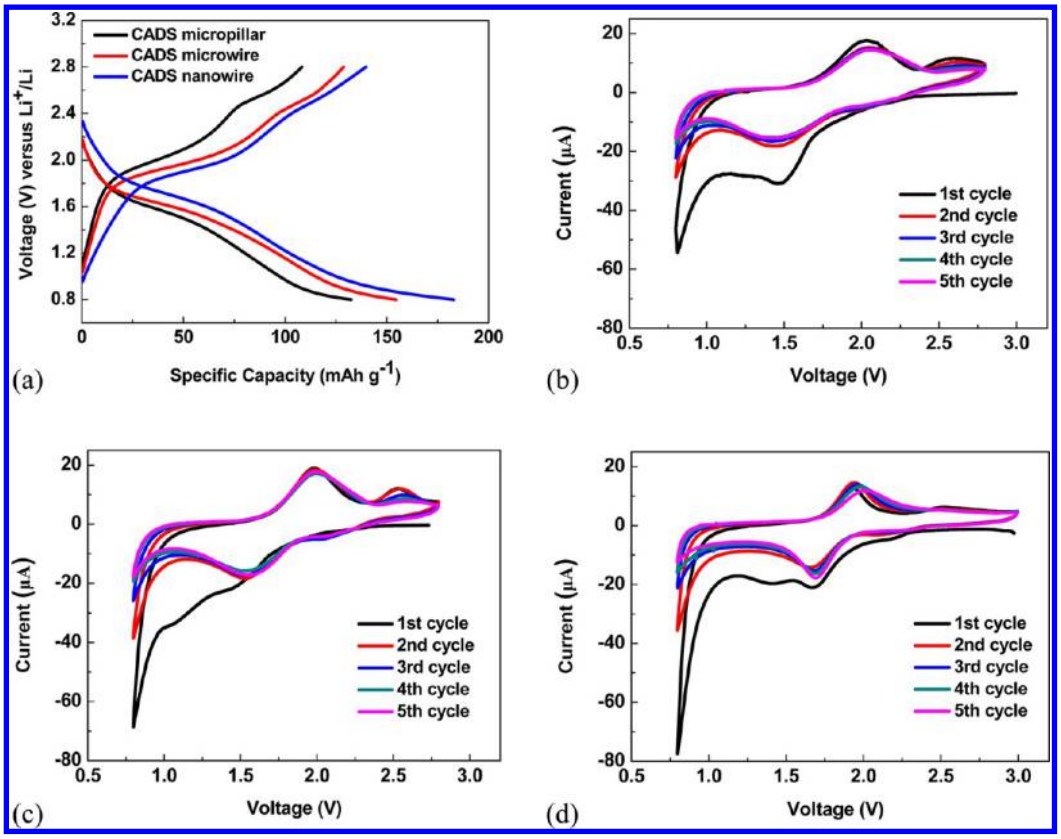

Figure 3. Electrochemical performance of CADS micropillar, CADS microwire, and CADS nanowire. (a) Charge and discharge curves of CADS micropillar, CADS microwire, and CADS nanowire for the second cycle; cyclic voltammograms for CADS micropillar (b), CADS microwire (c), and CADS nanowire (d).

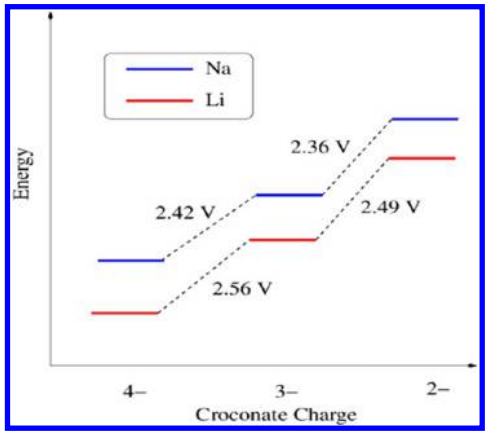

Figure 4. Calculated energy levels of NaCA and LiCA. Potentials shown are referenced to the Li electrode.

without corresponding cathodic peak is observed in the cyclic voltammograms of CADS micropillar, CADS microwire, and CADS nanowire. The sharp peak at 0.8 V becomes weaker after each cycle, suggesting that stable SEI layer is formed during the first cycle.

The cycling performance of CADS electrodes is shown in Figure 5a. The specific capacities of CADS micropillar, CADS microwire, and CADS nanowire decrease a little in the first 20 cycles, and then it becomes very stable for CADS micropillar, and even increases back to original capacity at 110 cycles for CADS nanowires, and slightly lower than initial capacity at 110 cycles for CADS microwires. This kind of cycling behavior is also observed in nano-Si/C composite.[32] As indicated by Figure 3b–d, the reductive peak at 0.8 V, corresponding to the formation of SEI layer, decays rapidly during the initial cycles, resulting in capacity decline. To identify the mechanism for capacity increase of CADS after 20 cycles, the charge/discharge profiles of CADS nanowire, CADS microwire, and CADS micropillar from 5th cycle to 30th cycle are shown in Supporting Information Figure S1. From the charge/discharge curves of CADS nanowires at different cycles in Supporting Information Figure S1a, it can be clearly observed that the lithiation plateau and delithiation plateau shift close to each other upon cycling, indicating smaller overpotential and faster kinetics. At initial cycles, the electrolyte does not fully penetrate to the entire electrode, leading to large overpotential and slow kinetics. Upon cycling, the large volume expansion and shrinkage of CADS increase the porosity of the CADS electrodes, allowing the electrolyte to penetrate the entire electrode, thus shortening the ion diffusion pathway and lowering the overpotential after 30 cycles. The fast kinetics enhances the utilization of organic electrode, resulting in increase of capacity. However, for microsize CADS electrode the large volume change also generates cracks, resulting in capacity decline in the initial cycles. The formation of cracks offsets the kinetic enhancement induced by electrolyte penetration so that the overpotential change from 5th cycle to 30th cycle is very small as evidenced by the little plateau shift in Supporting Information Figure S1b,c. The reversible capabilities of CADS micropillar, CADS microwire, and CADS nanowire measured at a current density of 0.2 C are 85, 132, and 177 mAh g^{-1}, respectively. CADS nanowire retains its initial capacity after 110 deep charge/discharge cycles.

dx.doi.org/10.1021/nl500026j | Nano Lett. 2014, 14, 1596–1602

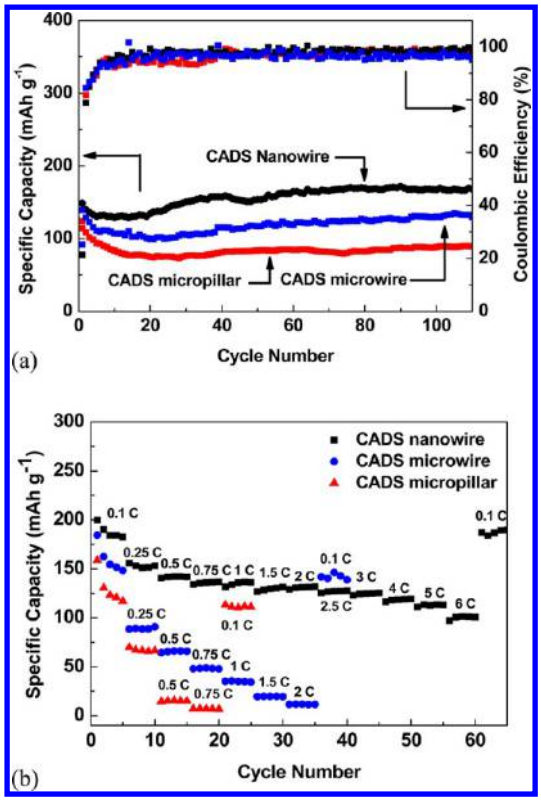

Figure 5. Cycle life (a) and rate capability (b) of CADS micropillar, CADS microwire, and CADS nanowire. (1 C is defined as 288 mA g^{-1}.)

Because CADS is an insulating material, lithium ions and electrons cannot be easily transported into the inside of bulk CADS material, but the smaller size and larger surface area of CADS nanowire enable more CADS to react with lithium ions, and lithium ions can quickly transfer to inside of CADS, so the specific capacity and rate capability of CADS nanowire are much higher than that of CADS micropillar and CADS microwire. The rate capability of CADS micropillar, CADS microwire, and CADS nanowire is shown in Figure 5b. With the current density increases from 0.1 to 0.75 C, the specific capacity of CADS micropillar decreases rapidly from 125 to 7 mAh g^{-1}. Although the capacity of CADS microwire is still 48 mAh g^{-1} at the current density of 0.75 C, the specific capacity of CADS microwire decreases from 160 to 11 mAh g^{-1} when the current density increases from 0.1 to 2 C, indicating the inferior rate performance of CADS microwire due to the large diameter (~4 μm). On the contrary, the smaller size and larger surface area of CADS nanowire can shorten the lithium ion diffusion length and enables better contact between CADS and conductive carbon. Therefore, CADS nanowire retains 50% of its initial capacity (200 mAh g^{-1}) subjected to the current density up to 6 C. After the current density returns to 0.1 C, the capacity of CADS nanowire recovers to its initial capacity immediately. Hence, from the electrochemical performance of CADS micropillar, CADS microwire, and CADS nanowire we can conclude that nanowire structure makes great contribution to the high capacity and high power density of CADS material.

The reaction kinetics of CADS materials was investigated using electrochemical impedance spectroscopy. The high-frequency semicircle represents interface resistance including contact impedance or SEI impedance as well as charge transfer impedance while the low frequency line stands for ion diffusion resistance. As shown in Figure 6, both the interface and diffusion impedances of CADS nanowire are much lower than

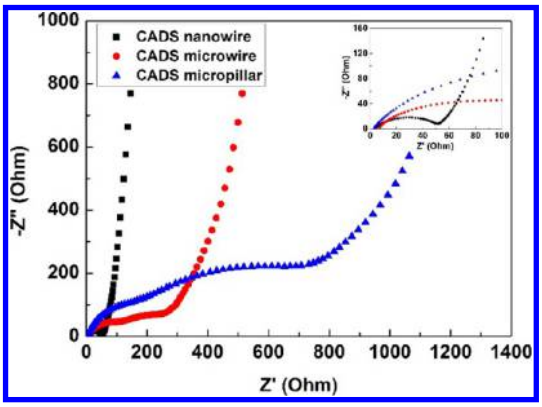

Figure 6. EIS spectra for CADS micropillar electrode, CADS microwire electrode, and CADS nanowire electrode. (The inset is magnification of the semicircle of CADS nanowire.)

that of CADS micropillar and CADS microwire, indicating the lower interface resistance and better kinetics of CADS nanowire. The interface resistance of CADS nanowire is about 50 Ω, while that for CADS micropillar electrode and CADS microwire electrode have much higher value of 300 and 750 Ω, respectively. The impedance results convince that the high capacity and superior rate capability of CADS nanowire is due to the large electrochemical reaction interface and short Li diffusion pathway.

The morphology of CADS micropillar, CADS microwire, and CADS nanowire after 110 cycles were investigated by SEM. As shown in Figure 7a, there are a number of microsize short rods around the large size CADS micropillar, demonstrating severe pulverization occurs after 110 charge/discharge cycles. The CADS microwires maintains its morphology after 110 cycles (Figure 7b), but a few short CADS rods and microcracks induced by the large strain during repeated charge/discharge cycles can still be observed. Different from CADS microwires, CADS nanowire preserves its morphology after 110 cycles in Figure 7c; no cracks and pulverization can be observed. The good morphology maintenance of CADS nanowires enables its high cycling stability.

In summary, during repeated lithiation/delithiation CADS will gradually convert to croconic acid dilithium salt through ion exchange (Scheme 2), as suggested by theoretical calculation and evidenced by the potential shift in CV scans and reduction of Na^+ concentration in cycled CADS electrode. More importantly, CADS nanowire with small size (150 nm) and large surface area can effectively avoid pulverization and enables stable contact between CADS and carbon black, providing high capacity, high rate capability, and long cycling stability. Because of the large size of CADS microwire, large volume change exists and leads to the formation of cracks and microcracks, as evidenced by SEM images of cycled CADS microwires. The microcracks that lose contact with carbon black are not electroative, resulting in capacity decline in the initial cycles. Therefore, nanosize CADS has much better electrochemical performance than microsize CADS.

The CADS wires with diameters from 10 μm to 150 nm were synthesized using a facile antisolvent crystallization method. The CADS nanowire with small diameter and large surface area shows high capacity, long cycle life, and excellent rate capability

dx.doi.org/10.1021/nl500026j | Nano Lett. 2014, 14, 1596−1602

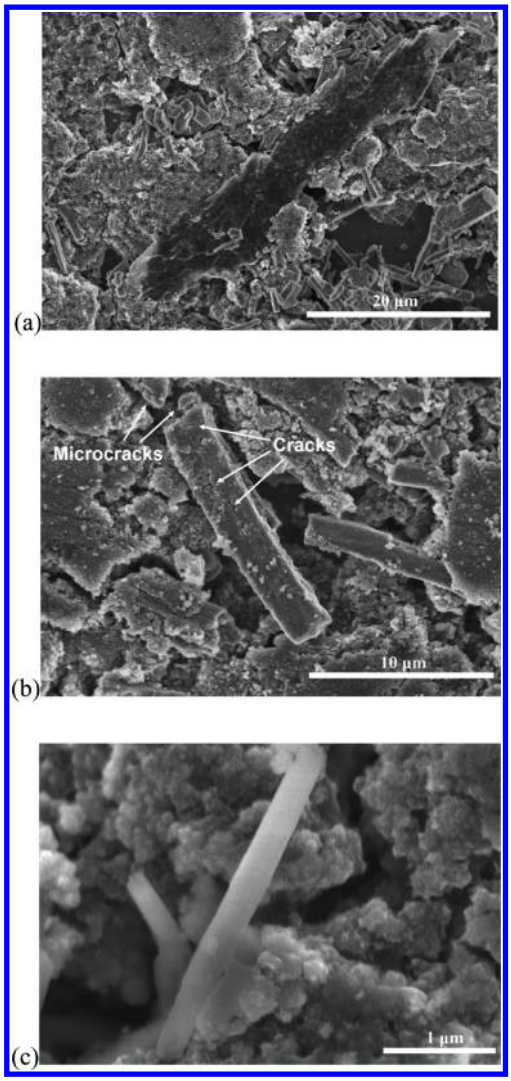

Figure 7. SEM images for CADS micropillar (a), CADS microwire (b), and CADS nanowire (c) after 100 cycles.

due to its short Li-ion and electron diffusion pathway, large surface area, and low strain. CADS nanowire can retain its initial capacity after 110 deep charge/discharge cycles at a low current density of 0.2 C, and deliver a high capacity of 100 mAh g^{-1} at 6 C. The theoretical calculation shows that the CADS gradually changes into more stable lithium croconate through ion exchange process during lithiation/delithiation. The ion exchange process is confirmed by ICP result, which shows the high content of lithium ion and low content of sodium ion in the cycled CADS electrode. Because the nano-organic material exhibits superior electrochemical performance, our research work paves the way for further improvement of organic battery performance in the future.

■ ASSOCIATED CONTENT

Supporting Information

Details of the synthesis, characterization, electrochemical measurements, and theoretical calculation. This material is available free of charge via the Internet at http://pubs.acs.org.

■ AUTHOR INFORMATION

Corresponding Authors

*E-mail: (H.H.) huixinhe@rutgers.edu.
*E-mail: (C.W.) cswang@umd.edu.

Author Contributions

§C.L. and R.H. contributed equally.

Notes

The authors declare no competing financial interest.

■ ACKNOWLEDGMENTS

This work was supported by the Army Research Office under Contract Nos. W911NF1110231 and NSF MRI-1039828. We acknowledge the support of the Maryland NanoCenter and its NispLab. The NispLab is supported in part by the NSF as a MRSEC Shared Experimental Facility. We acknowledge Junkai Hu and Professor Sang Bok Lee for their technique support.

■ REFERENCES

(1) Scrosati, B.; Hassoun, J.; Sun, Y. *Energy Environ. Sci.* **2011**, *4*, 3287−3295.
(2) Goodenough, J. B.; Kim, Y. *Chem. Mater.* **2010**, *22*, 587−603.
(3) Ellis, B. L.; Lee, K. T.; Nazar, L. F. *Chem. Mater.* **2010**, *22*, 691−714.
(4) Chung, S.; Bloking, J. T.; Chiang, Y. *Nat. Mater.* **2002**, *1*, 123−128.
(5) Kang, B.; Ceder, G. *Nature* **2009**, *458*, 190−193.
(6) Zhu, Y.; Xu, Y.; Liu, Y.; Luo, C.; Wang, C. *Nanoscale* **2013**, *5*, 780−787.
(7) Liang, Y.; Tao, Z.; Chen, J. *Adv. Energy Mater.* **2012**, *2*, 742−769.

Scheme 2. Schematic Illustration of Lithiation/De-Lithiation Mechanism for Croconic Acid Disodium Salt

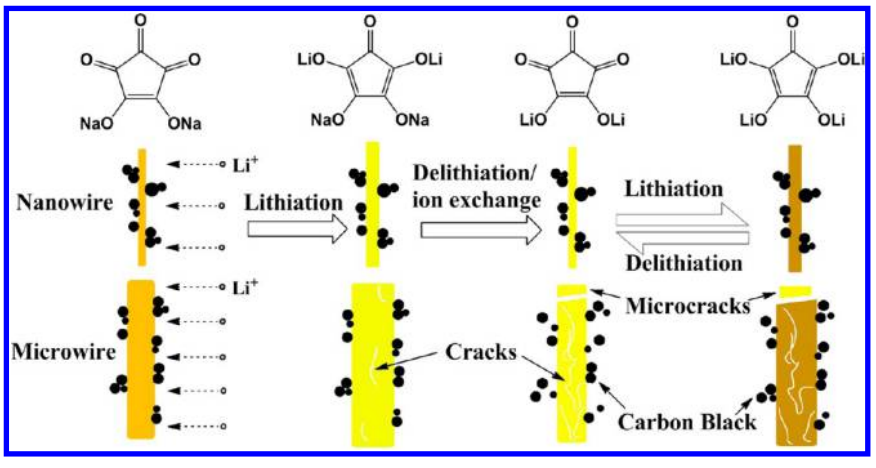

dx.doi.org/10.1021/nl500026j | *Nano Lett.* 2014, 14, 1596−1602

(8) Chen, H.; Armand, M.; Demailly, G.; Dolhem, F.; Poizot, P.; Tarascon, J. *ChemSusChem* **2008**, *1*, 348−355.
(9) Reddy, A. L. M.; Nagarajan, S.; Chumyim, P.; Gowda, S. R.; Pradhan, P.; Jadhav, S. R.; Dubey, M.; John, G.; Ajayan, P. M. *Sci. Rep.* **2012**, *2*, 960.
(10) Morita, Y.; Nishida, S.; Murata, T.; Moriguchi, M.; Ueda, A.; Satoh, M.; Arifuku, K.; Sato, K.; Takui, T. *Nat. Mater.* **2011**, *10*, 947−951.
(11) Han, X.; Chang, C.; Yuan, L.; Sun, T.; Sun, J. *Adv. Mater.* **2007**, *19*, 1616−1621.
(12) Song, Z.; Zhan, H.; Zhou, Y. *Angew. Chem., Int. Ed.* **2010**, *49*, 8444−8448.
(13) Song, Z.; Xu, T.; Gordin, M. L.; Jiang, Y.; Bae, I.; Xiao, Q.; Zhan, H.; Liu, J.; Wang, D. *Nano Lett.* **2012**, *12*, 2205−2211.
(14) Genorio, B.; Pirnat, K.; Cerc-Korosec, R.; Dominko, R.; Gaberscek, M. *Angew. Chem., Int. Ed.* **2010**, *49*, 7222−7224.
(15) Senoh, H.; Yao, M.; Sakaebe, H.; Yasuda, K.; Siroma, Z. *Electrochim. Acta* **2011**, *56*, 10145−10150.
(16) Geng, J.; Bonnet, J.; Renault, S.; Dolhem, F.; Poizot, P. *Energy Environ. Sci.* **2010**, *3*, 1929−1933.
(17) Han, X.; Qing, G.; Sun, J.; Sun, T. *Angew. Chem., Int. Ed.* **2012**, *51*, 5147−5151.
(18) Hanyu, Y.; Honma, I. *Sci. Rep.* **2012**, *2*, 453.
(19) Walker, W.; Grugeon, S.; Mentre, O.; Laruelle, S.; Tarascon, J.; Wudl, F. *J. Am. Chem. Soc.* **2010**, *132*, 6517−6523.
(20) Nokami, T.; Matsuo, T.; Inatomi, Y.; Hojo, N.; Tsukagoshi, T.; Yoshizawa, H.; Shimizu, A.; Kuramoto, H.; Komae, K.; Tsuyama, H.; Yoshida, J. *J. Am. Chem. Soc.* **2012**, *134*, 19694−19700.
(21) Kassam, A.; Burnell, D. J.; Dahn, J. R. *Electrochem. Solid-State Lett.* **2011**, *14*, A22−A23.
(22) Pirnat, K.; Dominko, R.; Cerc-Korosec, R.; Mali, G.; Genorio, B.; Gaberscek, M. *J. Power Sources* **2012**, *199*, 308−314.
(23) Xu, W.; Read, A.; Koech, P. K.; He, D.; Wang, C.; Xiao, J.; Padmaperuma, A. B.; Graff, G. L.; Liu, J.; Zhang, J. *J. Mater. Chem.* **2012**, *22*, 4032−4039.
(24) Pan, H.; Hu, Y.; Chen, L. *Energy Environ. Sci.* **2013**, *6*, 2338−2360.
(25) Zhao, L.; Zhao, J.; Hu, Y.; Li, H.; Zhou, Z.; Armand, M.; Chen, L. *Adv. Energy Mater.* **2012**, *2*, 962−965.
(26) Armand, M.; Grugeon, S.; Vezin, H.; Laruelle, S.; Ribière, P.; Poizot, P.; Tarascon, J. *Nat. Mater.* **2009**, *8*, 120−125.
(27) Suo, L.; Hu, Y.; Li, H.; Armand, M.; Chen, L. *Nat. Comm.* **2013**, *4*, 1481.
(28) Chen, H.; Armand, M.; Courty, M.; Jiang, M.; Grey, C. P.; Dolhem, F.; Tarascon, J.; Poizot, P. *J. Am. Chem. Soc.* **2009**, *131*, 8984−8988.
(29) Wang, S.; Wang, L.; Zhang, K.; Zhu, Z.; Tao, Z.; Chen, J. *Nano Lett.* **2013**, *13*, 4404−4409.
(30) Liu, H.; Li, J.; Lao, C.; Huang, C.; Li, Y.; Wang, Z.; Zhu, D. *Nanotechnology* **2007**, *18*, 495704.
(31) Hirai, K.; Ichitsubo, T.; Uda, T.; Miyazaki, A.; Yagi, S.; Matsubara, E. *Acta Mater.* **2008**, *56*, 1539−1545.
(32) Magasinski, A.; Dixon, P.; Hertzberg, B.; Kvit, A.; Ayala, J.; Yushin, G. *Nat. Mater.* **2010**, *9*, 353−358.